Tunable $(\delta\pi, \delta\pi)$-Type Antiferromagnetic Order in α-Fe(Te,Se) Superconductors

Wei Bao,[1,2,*] Y. Qiu,[3,4] Q. Huang,[3] M. A. Green,[3,4] P. Zajdel,[3,5] M. R. Fitzsimmons,[2] M. Zhernenkov,[2] S. Chang,[3] Minghu Fang,[6,7] B. Qian,[6] E. K. Vehstedt,[6] Jinhu Yang,[7] H. M. Pham,[8] L. Spinu,[8] and Z. Q. Mao[6]

[1]*Department of Physics, Renmin University of China, Beijing 100872, China*
[2]*Los Alamos National Laboratory, Los Alamos, New Mexico 87545, USA*
[3]*NIST Center for Neutron Research, National Institute of Standards and Technology, Gaithersburg, Maryland 20899, USA*
[4]*Department of Materials Science and Engineering, University of Maryland, College Park, Maryland 20742, USA*
[5]*Institute of Physics, University of Silesia, Uniwersytecka 4, 40-007 Katowice, Poland*
[6]*Department of Physics, Tulane University, New Orleans, Louisiana 70118, USA*
[7]*Department of Physics, Zhejiang University, Hangzhou 310027, China*
[8]*Department of Physics, University of New Orleans, New Orleans, Louisiana 70148, USA*

(Received 29 September 2008; published 17 June 2009)

The new α-Fe(Te,Se) superconductors share the common iron building block and ferminology with the LaFeAsO and $BaFe_2As_2$ families of superconductors. In contrast with the predicted commensurate spin-density-wave order at the nesting wave vector $(\pi, 0)$, a completely different magnetic order with a composition tunable propagation vector $(\delta\pi, \delta\pi)$ was determined for the parent compound $Fe_{1+y}Te$ in this powder and single-crystal neutron diffraction study. The new antiferromagnetic order survives as a short-range one even in the highest T_C sample. An alternative to the prevailing nesting Fermi surface mechanism is required to understand the latest family of ferrous superconductors.

DOI: 10.1103/PhysRevLett.102.247001 PACS numbers: 74.25.Ha, 61.05.fm, 74.70.−b, 75.30.Fv

The recently discovered ferrous superconductors differ from phonon-mediated conventional superconductors in an important way: when the nonmagnetic La in LaFeAs(O,F) is replaced by magnetic lanthanides, T_C increases from 26 K to as high as 55 K [1–4], in contrast to the breaking of the Cooper pairs by magnetic ions [5]. The La(O,F) ''charge reservoir'' layer turns out not to be a requirement for superconductivity and can be replaced by simple metal layers in $(Ba/Sr/Ca, K/Na)Fe_2As_2$ [6–9], or completely absent as shown more recently in the α phase of Fe(Se,Te) [10–12]. The common iron layer contributes dominantly to the electronic states at the Fermi level in these families of materials [13–17], which thus share similar quasi-two-dimensional Fermi surfaces with a nesting wave vector $(\pi, 0)$ in the reciprocal Fe square lattice. The antiferromagnetic order observed in the parent compounds of both the LaFeAsO [18] and $BaFe_2As_2$ [19] families of materials, Fig. 1(c), has been predicted by the nesting spin-density-wave (SDW) mechanism [20]. In view of insufficient electron-phonon coupling [21–23], spin excitations from the only known mode at $(\pi, 0)$ have been proposed as the bosonic ''glue'' mediating high T_C superconductivity in these ferrous materials [13–17,20].

However, the weak-coupling SDW mechanism critically depends on the matching electron and hole Fermi surfaces in the parent compounds [14]. The nesting condition is lost when adding electrons or holes to the systems [24]. This expectation is confirmed in systematic doping [25–27] and pressure studies [28], which show the destruction of the SDW order well before the optimal superconducting state is established. Moreover, despite the same $(\pi, 0)$ SDW order being predicted for α-FeTe in first-principles theory [17], we observed a completely different antiferromagnetic order with the in-plane propagation vector $(\delta\pi, \delta\pi)$ along the diagonal direction of the Fe ''square'' lattice, Fig. 1(b). The δ is tunable from an incommensurate 0.38 to the commensurate 0.5. Therefore, experimental results reported here call for a better understanding of the mechanism of magnetism and its role in superconductivity for the ferrous superconductors.

The single-phase $Fe(Te, Se)_z$ material in the tetragonal PbO structure exists in a composition range near $z = 1$ [29]. In this α phase [10–12] (called β phase in [29]), iron-chalcogen forms with the same edge-sharing antifluorite layers as found in the FeAs superconductors. The α-FeSe with the nominal composition $FeSe_{0.88}$ was recently reported to superconduct at $T_C \approx 8$ K [10], which increases to 27 K at 1.48 GPa [30]. The isovalent series $Fe(Te_{1-x}Se_x)_z$ in the α phase with nominal $z = 0.82$ has been synthesized, and the T_C is enhanced to 14 K at $x = 0.4$ at ambient pressure [11]. Similar results have also been reported for the nominal $z = 1$ series [12].

The end member α-$FeTe_z$ is not superconducting, and bulk measurements indicate a phase transition at $T_S \sim$ 60–75 K [11,12]. As a function of z, there exist two distinct types of transport behaviors in the low temperature phase: for $z \geq 0.90$ the samples change from a semiconductor to a metal, while for $z < 0.90$ the samples remain semiconducting [11]. Therefore, we selected a typical composition from each range of z for this study, $FeTe_{0.82}$ and $FeTe_{0.90}$. For superconducting α-$Fe(Te, Se)_z$, we chose the highest $T_C \approx 14$ K compound $Fe(Te_{0.6}Se_{0.4})_{0.82}$. The high-resolution powder diffraction spectra of polycrystalline samples, weighing 15–16 g, were measured with

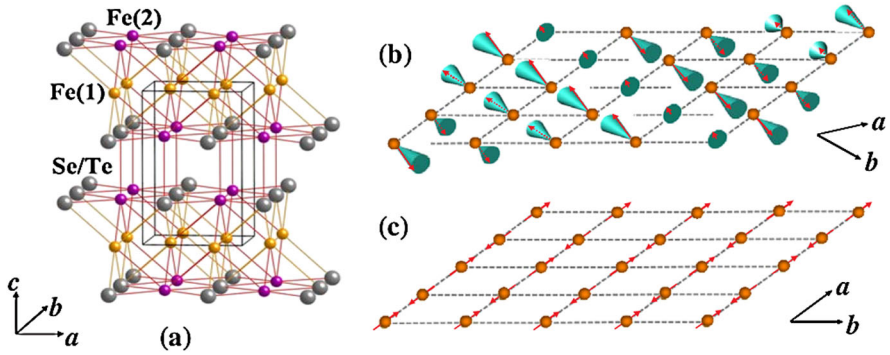

FIG. 1 (color online). (a) Crystal structure of α-Fe(Te,Se). Magnetic structures of (b) α-FeTe and (c) $BaFe_2As_2$ are shown in the *primitive* Fe square lattice for comparison. Note that the basal square lattice of the PbO unit cell in (a) is a $\sqrt{2} \times \sqrt{2}$ superlattice of that in (b).

neutrons of wavelength 2.0785 Å using BT1 at NIST (Fig. 2). See Ref. [31] for a table listing the refined parameters. The high-temperature phase of these samples indeed has the tetragonal $P4/nmm$ structure [10]; however, the chalcogen and Fe(1) sites of the PbO structure are fully occupied, and the excess Fe partially occupies the interstitial site Fe(2), see [31] and Fig. 1(a). Thus, the more appropriate formula for nominal α-$Fe(Te_{1-x}Se_x)_z$ is $Fe_{1+y}(Te_{1-x}Se_x)$.

While $Fe_{1.080}Te_{0.67}Se_{0.33}$ remains tetragonal in the superconducting state at 4 K [[31], Table I(c)], the parent compounds $Fe_{1.141}Te$ and $Fe_{1.076}Te$ experience a first-order magnetostructural transition, see Fig. 3, similar to that in $BaFe_2As_2$ [19]. The semiconducting $Fe_{1.141}Te$ distorts to an orthorhombic $Pmmn$ structure below $T_S \approx 63$ K, with the a axis expanding and the b axis contracting, Fig. 3(c) and [31], Table I(a). This results in the splitting of the $(h0k)$ Bragg peaks of the high-temperature structure, Fig. 2(b). The orthorhombic distortion here, however, does not double the unit cell, different from that observed in either the LaFeAsO [32] or $BaFe_2As_2$ [19]. The metallic $Fe_{1.076}Te$ has a monoclinic $P2_1/m$ structure below $T_S \approx 75$ K, [31], Table I(b). In addition to the differentiation of the a and b axis [Fig. 3(d)], the c axis rotates towards the a axis to $\beta \approx 89.2°$. Thus, the monoclinic distortion not only splits the (200) but also the (112) Bragg peak, Fig. 2(d). In the weaker first-order transition of $Fe_{1.141}Te$, a mixed phase exists in the pink-shaded region in Fig. 3(c). At 55 K upon warming, 85% of the sample is orthorhombic and 15% tetragonal. See Ref. [31] for the temperature dependence of distances and angles between various atoms.

The additional magnetic Bragg reflections of the monoclinic metal in Fig. 2(d) can be indexed by a commensurate magnetic wave vector $\mathbf{q} = (\frac{1}{2}0\frac{1}{2})$, as previously reported [33]. However, magnetic Bragg reflections of the orthorhombic semiconductor in Fig. 2(b) cannot be indexed by multiples of the nuclear unit cell. By performing *single-*

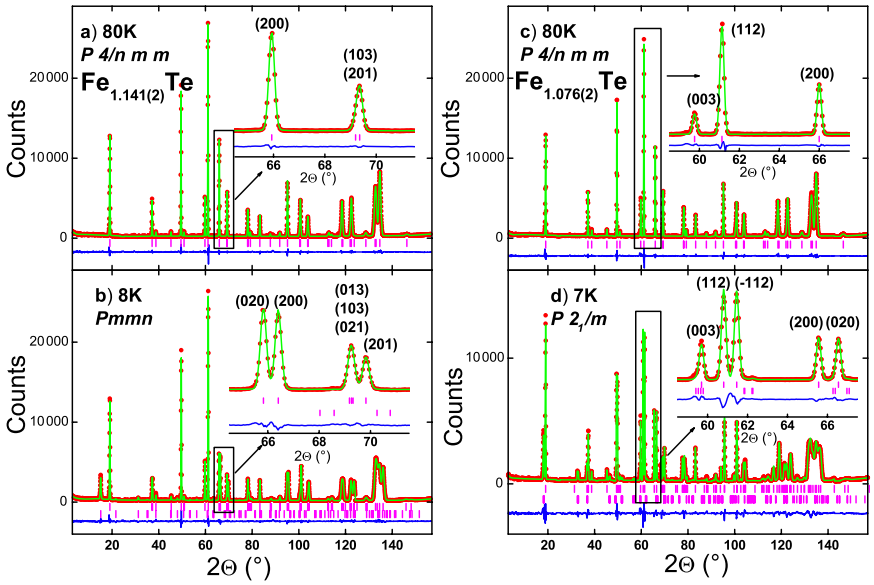

FIG. 2 (color online). Neutron powder diffraction spectra of $Fe_{1.141}Te$ and $Fe_{1.076}Te$ above and below the phase transition.

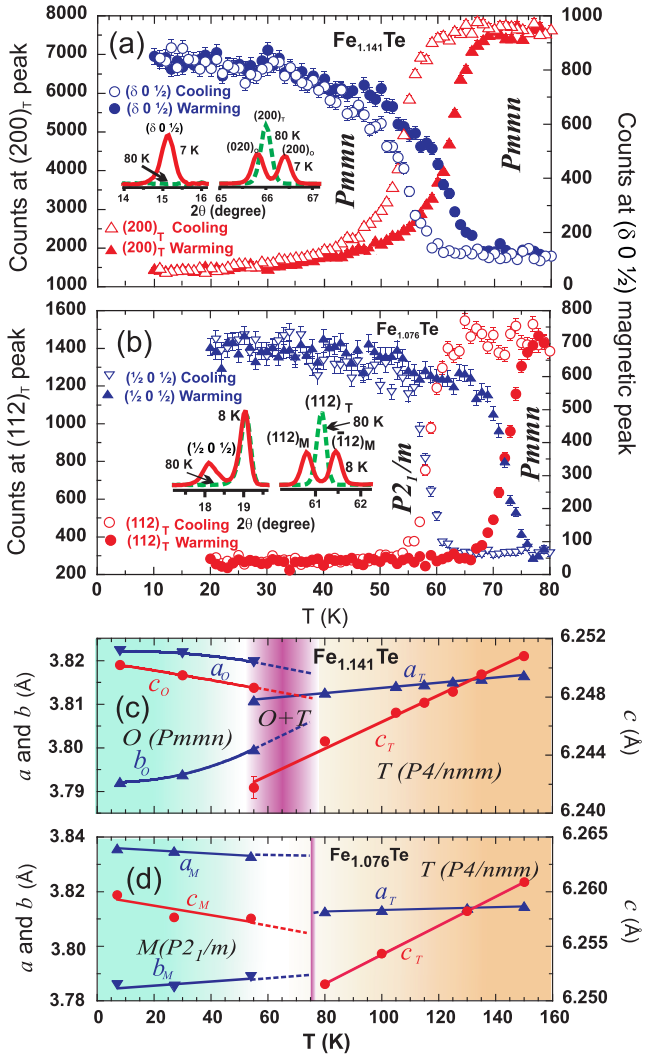

FIG. 3 (color online). (a),(b) The magnetic Bragg peak (δ, 0, 1/2) (blue symbols) and the splitting of the structural peak (200) or (112) of the tetragonal phase (red symbols) show the thermal hysteresis in the first-order transition. (c),(d) The lattice parameters through the transition.

crystal neutron diffraction using the triple-axis spectrometer BT9 at NIST, we determine the incommensurate magnetic wave vector $\mathbf{q} = (\pm\delta 0 \frac{1}{2})$, where $\delta \approx 0.380$, for $Fe_{1.141}Te$. The $\mathbf{q}$ determines that magnetic moments in each row along the b axis are parallel to each other. The rows of moments in an Fe plane modulate with the propagating vector $2\pi\delta/\mathbf{a}$, which is 45° away from that of previous FeAs materials, see Figs. 1(b) and 1(c). From one plane to the next along the c axis, magnetic moments simply alternate direction. In the same magnetostriction pattern as previously observed in the magnetic state of NdFeAsO [34] and $BaFe_2As_2$ [19], the lattice contracts in the b axis, along which the magnetic moments are parallel to each other, and it expands in the a and c axis, which are the directions of the antiferromagnetic alignment. Once again, the unusual coupling between the lattice and magnetic degrees of freedom is what expected from multiple d-orbital magnetism [15].

The observed magnetic powder spectra can be refined by a collinear sinusoid model,

$$\mathbf{M}^{l}(\mathbf{R}) = M_l \hat{\mathbf{b}} \cos(\mathbf{q}\cdot\mathbf{R} + \phi_{\mathbf{R}}), \tag{1}$$

where $\mathbf{R}$ is the position of the Fe, M_l the staggered magnetic moment, $\phi_{\mathbf{R}}$ the additional phase at the Fe site. The unit vector $\hat{\mathbf{b}}$ fixes the moment along the b-axis, and $\mathbf{q}$ is the observed magnetic wave vector. Refined magnetic parameters at low temperature are listed in Ref. [31] Table I(a) and (b). However, for an incommensurate $\mathbf{q}$, a spiral model with the moment rotating in the ac plane,

$$\mathbf{M}^{s}(\mathbf{R}) = M_s[\hat{\mathbf{a}}\cos(\mathbf{q}\cdot\mathbf{R} + \phi_{\mathbf{R}}) + \hat{\mathbf{c}}\sin(\mathbf{q}\cdot\mathbf{R} + \phi_{\mathbf{R}})], \tag{2}$$

offers an equivalent description of the *unpolarized* neutron diffraction results, with the relation between the respective neutron diffraction cross sections

$$2\sigma^{l}(\mathbf{Q})/\langle M_l\rangle^2 \equiv \sigma^{s}(\mathbf{Q})/\langle M_s\rangle^2. \tag{3}$$

Thus, any linear combination of Eqs. (1) and (2) is also an equivalent description. On the other hand, σ^l and σ^s are partial cross sections for different channels of *polarized* neutron scattering [35]. Therefore, they can be readily determined using polarized neutrons.

We measured a $Fe_{1.141}Te$ single-crystal sample, aligned in the ($h0l$) horizontal scattering plane, using polarized neutron spectrometer Asterix at the Lujan Center of LANL. The neutron spin is controlled to align either perpendicular to the ($h0l$) plane (VF) or parallel to the momentum transfer (HF). All four channels ($++$, $+-$, $-+$, $--$) in both the VF and HF configurations were measured for the (001) and $(\delta 0 \frac{1}{2})$ Bragg peaks. The flipping ratio of the instrument is 10.3 as measured at the nuclear (001) peak. The $(\delta 0 \frac{1}{2})$ is proved magnetic by the spin-flip scattering in HF. The normalized intensity of $(\delta 0 \frac{1}{2})$ in VF is 8.24(28) in the non-spin-flip (NSF) channels, and 4.13(20) in the spin-flip (SF) channels. After correcting for the finite flipping ratio of the instrument, we obtained $\sigma^l/\sigma^s \equiv I_{\mathrm{NSF}}/I_{\mathrm{SF}} = 7.91(27)/3.37(16)$. Therefore, the incommensurate magnetic structure for $Fe_{1.141}Te$ is

$$\begin{aligned}\mathbf{M}(\mathbf{R}) &= \mathbf{M}^{l} + \mathbf{M}^{s} \\ &= M[w\hat{\mathbf{b}}\cos(\mathbf{q}\cdot\mathbf{R} + \phi_{\mathbf{R}} + \psi) + \hat{\mathbf{a}}\cos(\mathbf{q}\cdot\mathbf{R} \\ &\quad + \phi_{\mathbf{R}}) + \hat{\mathbf{c}}\sin(\mathbf{q}\cdot\mathbf{R} + \phi_{\mathbf{R}})],\end{aligned} \tag{4}$$

where $w \equiv \sqrt{2\sigma^l/\sigma^s} = 2.17(6)$, $M = M_l/\sqrt{2+w^2} = 0.76(2)\mu_B$/Fe and ψ is an arbitrary phase between the spiral and the sinusoidal components; see Fig. 1(b).

To understand whether the incommensurate magnetic structure in the orthorhombic semiconducting phase is locked or tunable, we examined another sample

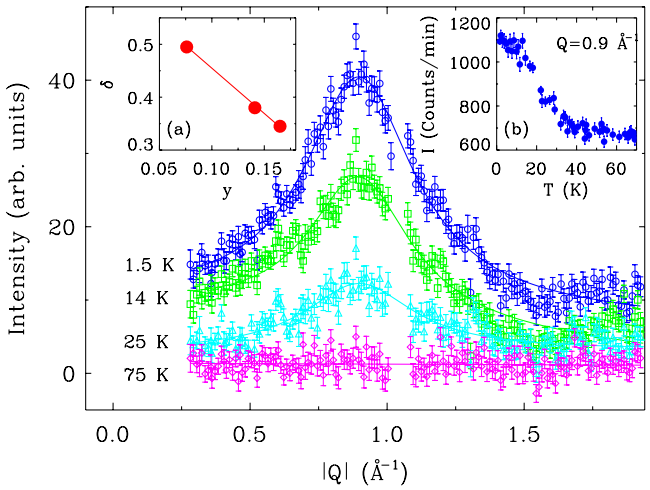

FIG. 4 (color online). Short-range magnetic order in superconducting $Fe_{1.080}Te_{0.67}Se_{0.33}$. The peak intensity as a function of temperature is shown in inset (b). Inset (a) shows the incommensurability δ as a function of y for $Fe_{1+y}Te$.

$Fe_{1.165(3)}Te$ by powder diffraction at BT1, [31], Table I(d). The incommensurability is greatly affected and measures at $\delta = 0.346$, despite no appreciable differences in either the moment or the phase ϕ from $Fe_{1.141}Te$ in [31], Table I(a). Thus, δ can be tuned by varying the excess Fe in the orthorhombic phase, and it reaches a commensurate value $\frac{1}{2}$ for the composition $Fe_{1.076}Te$ in the metallic monoclinic phase with less excess iron, see inset (a) of Fig. 4.

Having unveiled a tunable $(\delta\pi, \delta\pi)$-type of antiferromagnetic order in the parent compound $Fe_{1+y}Te$, it is natural to ask whether the new magnetic order survives in the optimal T_C superconducting sample $Fe_{1.080}Te_{0.67}Se_{0.33}$. While there is neither long-range magnetic order nor structural transition, we observed pronounced short-range quasielastic magnetic scattering at the incommensurate wave vector $(0.438, 0, \frac{1}{2})$, Fig. 4, using SPINS at NIST. The temperature insensitive half-width-at-the-half-maximum 0.25 Å^{-1} indicates a short magnetic correlation length of 4 Å, approximately only two nearest-neighbor Fe spacings. The concave shape of the peak intensity as a function of temperature in inset (b) indicates the expected diffusive nature of the short-range magnetic correlations. This is very different from the case of the $(\pi, 0)$ SDW which is completely suppressed in the optimal T_C FeAs samples [18,22,25,27].

To summarize, the α-Fe(Te,Se) shares a common electronic structure with the previously reported FeAs-based superconductor systems. Though the same $(\pi, 0)$ SDW order has been predicted [17], we show the presence of a fundamentally different $(\delta\pi, \delta\pi)$ antiferromagnetic order which propagates along the diagonal direction. The incommensurability δ in the orthorhombic semiconducting phase is easily tunable with excess Fe and locks into a commensurate $\frac{1}{2}$ in the monoclinic metallic phase. This magnetic order, which survives as short-range order even in the optimal superconducting state, cannot be the result of Fermi surface nesting, which is along the $(\pi, 0)$ direction and delicately depends on electronic band filling for its existence.

Work at LANL was supported by the DOE-OS-BES; at Tulane by the NSF grant DMR-0645305, the DOE DE-FG02-07ER46358 and the Research Corp.; at ZU by NBRP of China (No. 2006CB01003, 2009CB929104) and the PCSIRT of the MOE of China (IRT0754); at UNO by DARPA Grant No. HR0011-07-1-0031. SPINS is in part supported by NSF under Agreement DMR-0454672.

*wbao@ruc.edu.cn

[1] Y. Kamihara *et al.*, J. Am. Chem. Soc. **130**, 3296 (2008).
[2] X. H. Chen *et al.*, Nature (London) **453**, 761 (2008).
[3] G. F. Chen *et al.*, Phys. Rev. Lett. **100**, 247002 (2008).
[4] Z. A. Ren *et al.*, Chin. Phys. Lett. **25**, 2215 (2008).
[5] A. A. Abrikosov and L. P. Gorkov, Zh. Eksp. Teor. Fiz. **39**, 1781 (1960).
[6] M. Rotter *et al.*, Phys. Rev. Lett. **101**, 107006 (2008).
[7] G. F. Chen *et al.*, Chin. Phys. Lett. **25**, 3403 (2008).
[8] K. Sasmal *et al.*, Phys. Rev. Lett. **101**, 107007 (2008).
[9] G. Wu *et al.*, J. Phys. Condens. Matter **20**, 422201 (2008).
[10] F.-C. Hsu *et al.*, Proc. Natl. Acad. Sci. U.S.A. **105**, 14 262 (2008).
[11] M. Fang *et al.*, Phys. Rev. B **78**, 224503 (2008).
[12] K.-W. Yeh *et al.*, Europhys. Lett. **84**, 37 002 (2008).
[13] K. Haule *et al.*, Phys. Rev. Lett. **100**, 226402 (2008).
[14] I. I. Mazin *et al.*, Phys. Rev. Lett. **101**, 057003 (2008).
[15] T. Yildirim, Phys. Rev. Lett. **101**, 057010 (2008).
[16] I. A. Nekrasov *et al.*, JETP Lett. **88**, 144 (2008).
[17] A. Subedi *et al.*, Phys. Rev. B **78**, 134514 (2008).
[18] C. de la Cruz *et al.*, Nature (London) **453**, 899 (2008).
[19] Q. Huang *et al.*, Phys. Rev. Lett. **101**, 257003 (2008).
[20] F. Ma and Z. Y. Lu, Phys. Rev. B **78**, 033111 (2008); J. Dong *et al.*, Europhys. Lett. **83**, 27 006 (2008).
[21] L. Boeri *et al.*, Phys. Rev. Lett. **101**, 026403 (2008).
[22] Y. Qiu *et al.*, Phys. Rev. B **78**, 052508 (2008).
[23] A. D. Christianson *et al.*, Phys. Rev. Lett. **101**, 157004 (2008); R. Mittal *et al.*, Phys. Rev. B **78**, 104514 (2008).
[24] Z. P. Yin *et al.*, Phys. Rev. Lett. **101**, 047001 (2008).
[25] J. Zhao *et al.*, Nature Mater. **7**, 953 (2008); H. Luetkens *et al.*, *ibid.* **8**, 305 (2009).
[26] S. Margadonna *et al.*, Phys. Rev. B **79**, 014503 (2009).
[27] H. Chen *et al.*, Europhys. Lett. **85**, 17 006 (2009).
[28] A. Kreyssig *et al.*, Phys. Rev. B **78**, 184517 (2008).
[29] W. Schuster *et al.*, Monat. für Chem. **110**, 1153 (1979).
[30] Y. Mizuguchi *et al.*, Appl. Phys. Lett. **93**, 152505 (2008).
[31] See EPAPS Document No. E-PRLTAO-103-063927 for the refined parameters. For more information on EPAPS, see http://www.aip.org/pubservs/epaps.html.
[32] T. Nomura *et al.*, Supercond. Sci. Technol. **21**, 125028 (2008).
[33] D. Fruchart *et al.*, Mater. Res. Bull. **10**, 169 (1975).
[34] Y. Qiu *et al.*, Phys. Rev. Lett. **101**, 257002 (2008).
[35] R. M. Moon *et al.*, Phys. Rev. **181**, 920 (1969).